

Spherical Wave and Plane Wave Propagators

Charles L. Rino

<http://chuckrino.com/wordpress/>

February 13, 2011

Abstract

This paper explores the equivalence between spherical wave and plane wave propagators. Spherical wave propagators are intimately part of diffraction and boundary scattering theory. Consequently they are used almost exclusively in introductory presentations of electromagnetic theory. However, equivalent representations can be constructed from superpositions of propagating plane waves. This leads to two different approaches to diffraction theory. Spherical wave computations are initiated by induced point sources. Plane wave computations are initiated by an equivalent aperture plane field. Subsequent propagation can be computed with Fourier transformations. Sampling requirements ultimately limit the utility Fourier domain computations. Examples are presented.

1 Introduction

Radio frequency (RF) and optical remote sensing applications exploit diverse technologies, but the essential underlying physics is captured by the scalar time-harmonic form of the Helmholtz equation,

$$\nabla^2\psi(\mathbf{r}) + k^2\psi(\mathbf{r}) = 0, \quad (1)$$

where $\psi(\mathbf{r})$ is the complex field, $k = 2\pi f\bar{n}/c = 2\pi/\lambda$ with f , λ , \bar{n} , and c representing frequency, wavelength, refractive index, and the velocity of light, respectively. Green's theorem facilitates the construction of solutions to (1) as superpositions of spherical waves emanating from induced sources on boundary surfaces that isolate material regions in the propagation space. Kong emphasized this time-honored superposition principle by referring to his development of EM boundary scattering theory as the mathematical formulation of Huygen's principle, [1, Chapter 5.3]. However, in most practical problems the source region can be isolated from a source-free region by a bounding plane. In the source-free region beyond the bounding plane, (1) admits an exact solution as a superposition of plane waves. The propagating plane waves are initiated by a spectral decomposition of the field in the bounding plane. Thus, observable

fields beyond their source region can be computed as a superposition of spherical waves emanating from singular sources or as a superposition of plane waves emanating from the field in a bounding plane.

Much of our understanding of propagation, diffraction, and scattering phenomena comes from approximations that make the propagating wave fields easier to analyze. Examples include the Fraunhofer and Fresnel approximations and the Fourier-transform relation between the aperture stop area and the point-spread function in the focal plane of a lens system. Inhomogeneous but transparent structure in the propagation region can be accommodated by replacing the right-hand side of (1) with the distributed source term

$$S(\mathbf{r})\psi(\mathbf{r}) = -2k^2 (\overline{\delta n}(\mathbf{r})/\bar{n})\psi(\mathbf{r}). \quad (2)$$

The refractive index variation has been incorporated by using the following definition of the refractive index:

$$n(\mathbf{r}) = (\bar{n} + \overline{\delta n}(\mathbf{r})). \quad (3)$$

To the extent that backscatter induced by $\overline{\delta n}(\mathbf{r})$ has a negligible effect on the wavefield propagating away from the initiation plane, the same free-space propagator interacts continuously with the effective source term.[2, Chapters 2 and 3] With the introduction of a varying refractive index, ray optics can be added to the approximate procedures that simplify the computation of propagating wavefields.

Often the fields of interest are sufficiently removed from the source region that angular displacements about the observation point are small compared to the propagation distance. One can exploit this constraint either by approximating the spherical wave radii to the point of observation or by approximating the plane-wave propagation operator. Approximating the propagation operator leads to the parabolic wave equation (PWE), which is well known in optics, RF, and acoustics.[3] The utility of the method comes from the fact that sampling requirements driven by the angular extent of a cone that captures the propagating waves. The sample intervals are much larger than the operating wavelength.

This paper reviews the mathematical equivalence between plane-wave and spherical-wave propagation computations with emphasis on numerical computation based on full-wave propagation in source-free regions. The theoretical support for what amounts to the theory of diffraction is well articulated in the seminal expose by Born and Wolf.[4]. However, modern computation capabilities bring more rigorous theoretical results into the “easier to analyze” regime. The diffraction operator is a case in point. It can be evaluated by using two-dimensional discrete Fourier transforms with no approximation other than those imposed by sampling.

The demonstration of equivalence between spherical-wave and plane-wave formulations would be of purely academic interest if alternative computational procedures did not provide computational or analytic advantages. The most demanding computation is the propagation of the field in the aperture stop

plane of a focusing lens system through the focus and beyond. It has already been noted that computation requirements are driven by the angular spread of the aperture wavefield distribution. However, one finds that the angular spread of a converging spherical wave subtends more than 50% of the diffraction limit, which is well beyond narrow-angle scatter. The equivalent Huygens-Fresnel construction has the same sampling requirements, but the concentration of the field near the focus makes adequate local sampling at optical wavelengths feasible. A full diffraction computation at 500 GHz is demonstrated, without special procedures to manage memory or to take advantage of the small support of the field as the focal point is approached.

2 Background

The common starting point for theoretical development is the scalar Helmholtz equation, which as already been introduced. Equation (2.2) in Rino [2] is the vector form of (1). Equation (3-8) in Goodman [5] is the time-domain form of the parent equation that leads to (1). The derivation of the modified form of the Helmholtz equation neglects the term, $\nabla(\mathbf{E} \cdot \nabla \ln n)$. Equation (3-13) in Goodman [5] is equivalent to (1) when the source term is included. In all cases, the time variation of the complex fields, $\exp\{-2\pi i f t\}$, is implicit. The treatment here is for fully coherent wavefields.

2.1 Boundary Integral Representations

As noted in the introduction, boundary integral representations are used to characterize the interaction of EM waves with material objects and boundary surfaces. The development in Goodman [5] follows Born and Wolf [4], which starts with the scalar boundary-integral representation

$$\psi(\mathbf{r}) = \iint_{\Sigma} \left[\frac{\partial \psi(\mathbf{r}_s)}{\partial N} G(\mathbf{r}, \mathbf{r}_s) + \psi(\mathbf{r}_s) \frac{\partial G(\mathbf{r}, \mathbf{r}_s)}{\partial N} \right] ds. \quad (4)$$

In (4), $\psi(\mathbf{r})$ represents the complex field in the unbounded region outside the boundary Σ , and

$$G(\mathbf{r}, \mathbf{r}_s) = \frac{\exp\{ik|\mathbf{r} - \mathbf{r}_s|\}}{|\mathbf{r} - \mathbf{r}_s|}, \quad (5)$$

is the scalar Green function. One can show that $\psi(\mathbf{r})$ is a formal solution to Helmholtz equation by virtue of the singular behavior of the Green function as $\mathbf{r} \rightarrow \mathbf{r}_s$. The Green function and its normal derivative propagate induced fields on the boundary surfaces throughout the exterior region as spherical waves. A radiation condition eliminates contributions from the outer boundary that closes the Green theorem surface.

A self-consistent determination of the induced boundary fields requires detailed knowledge of the electric properties of the medium inside the boundary as well as the boundary surface geometry. For perfectly conducting surfaces,

the boundary integral can be manipulated as written to determine the induced fields. Either the field or its normal derivative is forced to be zero on the boundary. Equations that can be solved for the unknown source fields can be obtained by taking the limit as $\mathbf{r} \rightarrow \mathbf{r}_s$, but in doing so one must accommodate the singular behavior of the Green function and its normal derivative. However this is done, stable results demand sub-wavelength sampling and extreme care in their formulation. Most practical applications of boundary-integral representations approximate the induced fields.

For reference, the essential elements of the theory of diffraction as it is developed for optical systems are captured by the Dirichlet integral representation

$$\psi(\mathbf{r}) = \iint_{\Sigma} U(\mathbf{r}_s) G(\mathbf{r}, \mathbf{r}_s) ds, \quad (6)$$

where $U(\mathbf{r}_s)$ is a source function on a prescribed surface. If $U(\mathbf{r}_s)$ represents an evolving spherical wavefront, (6) is a mathematical statement of the Huygens-Fresnel construction. The equivalence that will be established later is readily generalized to forms of the theory that incorporate the derivative (Neumann) term and extensions to vector fields.

2.2 The Forward Approximation

The theoretical development in [2, Chapter 2] avoids an explicit treatment of scattering theory by exploiting the fact that propagating waves, however they are initiated, are highly directed but not necessarily confined to a narrow cone of scattering angles. This is made explicit by showing that (1) with the source term admits an equivalent representation as a pair of coupled first-order differential equations. The coupled equations individually characterize wave fields that propagate in opposite directions with respect to a prescribed reference axis. In the absence of the weakly inhomogeneous structure that couples the equations, the solutions are uncoupled and solve (1) exactly. A unidirectional source excites waves propagating in the opposite direction only through scattering interactions within the medium, but these scattering interactions have a negligible effect on the dominant forward propagating wavefield.

The result is a first-order differential equation called the forward propagation equation (FPE). The following scalar FPE fully characterizes propagation in an unbounded weakly inhomogeneous medium:

$$\frac{\partial \psi(x, \varsigma)}{\partial x} = \Theta \psi(x, \varsigma) + ikS(x, \varsigma; \lambda) \psi(x, \varsigma). \quad (7)$$

In (7) $\psi(x, \varsigma)$ represents the complex wave field in a rectangular coordinate system with x the propagation reference axis and ς a position vector in the plane normal to the x direction. The source term has already been introduced. The leading term in (7) represents the propagation of a coherent monochromatic wave field in a homogeneous medium. The exact form of the propagation

operator is

$$\Theta\psi(x, \varsigma) = \iint \widehat{\psi}(x_0, \kappa) \exp\{\pm ikg(\kappa)(x - x_0)\} \\ \times \exp\{i\kappa \cdot \varsigma\} \frac{d\kappa}{(2\pi)^2}. \quad (8)$$

The complex field, $\widehat{\psi}(x_0, \kappa)$, is the two-dimensional Fourier transform of the field in the plane at $x = x_0$

$$\widehat{\psi}(x_0, \kappa) = \iint \psi(x_0, \varsigma) \exp\{-i\kappa \cdot \varsigma\} d\varsigma, \quad (9)$$

and

$$g(\kappa) = \begin{cases} \sqrt{1 - (\kappa/k)^2} & \text{for } \kappa \leq k \\ i\sqrt{(\kappa/k)^2 - 1} & \text{for } \kappa > k \end{cases}. \quad (10)$$

Irrespective of how the FPE was derived, one can readily verify by direct substitution that (8) satisfies (1). Thus, solutions to the FPE in a homogeneous medium are exact solutions to the homogeneous Helmholtz equation. The unnumbered equation in Section 3.10.4 of Goodman [5] is equivalent to (8),¹ but Goodman does not use it in his subsequent developments.

2.2.1 Narrow-angle scatter

For numerical integration of the FPE, the narrow-angle approximation is neither required nor advantageous. However, the narrow-angle scatter approximation is essential for analytic computations. When the spectral content of the field $\widehat{\psi}(x_0, \kappa)$ is well contained within the disk defined by $\kappa = k$, one can use the approximation

$$g(\kappa) \cong 1 - (\kappa/k)^2 / 2. \quad (11)$$

The Formal equivalence of multiplication in the Fourier domain by powers of κ and derivatives of the same order in the spatial domain leads to the following formal definition of the diffraction-operator and the parabolic approximation:

$$ik\Theta = ik\sqrt{1 + \nabla_{\perp}/k^2} \\ \cong ik + i\nabla_{\perp}/(2k). \quad (12)$$

The parabolic approximation (7), namely

$$\frac{\partial U(x, \varsigma)}{\partial x} = i\nabla_{\perp}U(x, \varsigma)/2k + ik\delta n(x, \varsigma)U(x, \varsigma), \quad (13)$$

is obtained by applying (12) and performing some straightforward manipulations. The PWE solutions apply to the modified field

¹In Rino [2] the propagator is defined in terms of spatial frequencies represented by $\kappa = [\kappa_y, \kappa_z]$ where $\kappa_y = 2\pi/L$ rather than spatial frequencies.

$$U(x, \varsigma) = \psi(x, \varsigma) \exp\{-ikx\}, \quad (14)$$

although removal of $\exp\{-ikx\}$ does not influence computational requirements.

2.3 Ray Optics

The theory of ray optics is derived by approximating vector fields by products of the form $\mathbf{A}(x, \varsigma) \exp\{ik\phi(x, \varsigma)\}$. The refractive index is treated as a continuous variable. When the refractive index gradients are small, which is a necessary condition for weakly inhomogeneous media, the evolving field structure can be characterized by propagation along geometric ray paths. The ray trajectories are defined by position-dependent vectors $\mathbf{r}(s)$, where s is the distance along the ray. The vector $\mathbf{r}(s)$ is constrained locally by two orthogonal vectors, namely the unit vector \mathbf{s} tangent to the ray at $\mathbf{r}(s)$ and the curvature vector $\boldsymbol{\varkappa} = d\mathbf{s}/ds$, which is normal to \mathbf{s} . The ray trajectory in the medium must satisfy the ray equation

$$n\boldsymbol{\varkappa} + \frac{dn}{ds}\mathbf{s} = \nabla n. \quad (15)$$

This equation can be derived from (13) by assigning the phase variation

$$\exp\{ik\phi(x, \varsigma)\}$$

to $U(x, \varsigma)$ [3, Chapter 5.2]. This is the basis for the earlier claim that ray optics in unbounded media is contained in the broader class solutions to the FPE. Note that aside from the wavelength dependence of the refractive index, the ray trajectories are wavelength independent.

2.4 Optical Lens Systems

Optical lens systems require special treatment for two reasons. First, a lens is defined by discontinuous boundaries, which often have discontinuous normal derivatives as well. Thus, an optical lens cannot be part of a weakly inhomogeneous medium. Second, the diffraction effects that limit the resolution of optical systems ultimately must be reincorporated into the analyses. A highly simplified lens system is used here to illustrate the use of ray optics to approximate a starting field for Fourier-domain computation.

Consider a representative lens system constructed from a colinear arrangement of homogeneous radially symmetric lens objects. For simplicity, lens objects will be confined to closed volumes circumscribed by intersecting spherical segments. As already noted, boundary scattering theory tells us that the transmission and scattering (reflecting) properties of lens objects are determined by the shape of the defining boundary surfaces and the constitutive properties of the lens material. The dielectric properties are defined by a frequency-dependent refractive index. From ray theory it follows that ray paths within homogeneous lens objects are straight lines.²

²For this development only monochromatic radiation will be considered.

A planar boundary admits an exact solution that can be constructed by applying Snell's law to determine the wavefront propagation directions on either side of the boundary:

$$\frac{\sin \theta_1}{\sin \theta_2} = \frac{n_2}{n_1}. \quad (16)$$

If the boundary variations are smooth enough, the boundary conditions are approximated by applying Snell's law with respect to the surface normal. The implicit assumption here is that the lens system is sufficiently uniform that rays can be approximated by straight lines inside lens objects. Thus, ray segments can be defined by unit vectors, \mathbf{u}_i , where i corresponds to the side of the boundary in which the ray is defined. Let \mathbf{u}_n represent a unit vector normal to the surface. At the boundary

$$\mathbf{u}_i \cdot \mathbf{u}_n = \cos \theta_1,$$

which defines $\sin \theta_1$. Snell's law defines $\sin \theta_2$, which is measured with respect to $-\mathbf{u}_n$. The following pair of equations define the continuation of ray trajectories within lens objects:

$$-\mathbf{u}_n \cdot \mathbf{u}_2 = \sqrt{1 - \sin^2 \theta_2} \quad (17)$$

$$-\mathbf{u}_n \times \mathbf{u}_2 = \sin \theta_2 \quad (18)$$

Knowing \mathbf{u}_2 , one can calculate the intersection of the ray with the opposite lens cap. The process can then be repeated to determine the direction of the rays exiting the lens object. There are many utilities available that will perform completely general ray analyses of lens systems and report the results graphically or in tabular form. However, the simpler formulation is useful for illustrative purposes. Figure 1 shows the evolution of a bundle of paraxial rays through a bispherical lens. The cap radii are 120 mm. The lens thickness is 10 mm. The refractive index at $.46 \mu$ is 1.62. The red pentagram show the nominal location of the focus calculated from the lens equation

$$\frac{1}{f} = (n - 1) \left(\frac{1}{r_1} - \frac{1}{r_2} + \frac{(n - 1)}{n} \frac{d}{r_1 r_2} \right), \quad (19)$$

where $\pm r_n$ is the positive convex radius of curvature of the lens faces, and d is the thickness of the lens along the central ray.

2.4.1 Field Estimation

The modified ray-optics construction just described is the only practical way to compute an optical field in the aperture stop of a lens system. Consider the normal plane at $x = 10$ mm. The optical path is defined as the ray-path integral weighted by the refractive index:

$$s = \oint n ds = \sum_i n_i s_i. \quad (20)$$

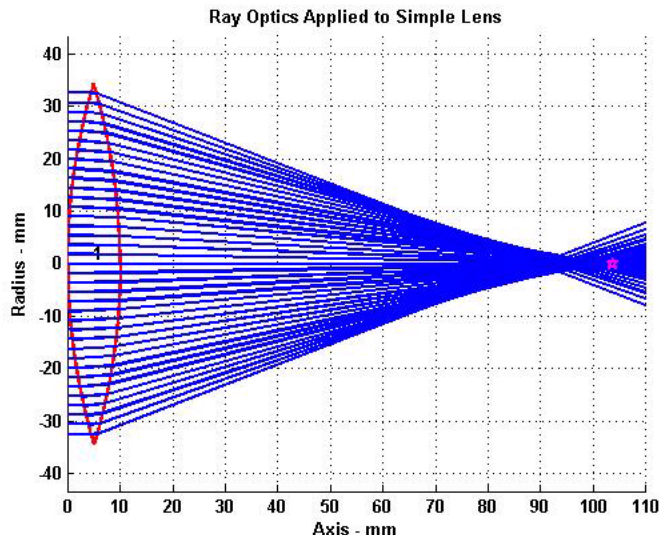


Figure 1: Vertical cross section of the ray-trace evolution of a parallel bundle of rays interacting with a bispherical lens. The red pentagram shows the predicted focal point.

The summation is over the three straight-line paths that connect points in the entrance plane to points in the exit plane. The complex field in the vertical plane has the form

$$\psi(x, \zeta') = A(x, \zeta') \exp\{iks(\zeta')\}. \quad (21)$$

The amplitude weighting accounts for the increased field intensity necessary to conserve energy as the field intensity becomes more concentrated, but that small correction will be ignored here. Figure 2 shows the optical path computed at the exit plane of the lens object shown in Figure 1. An eighth-order polynomial fit was used to approximate the optical path.

Figure (3) shows a purely quadratic phase variation overlaid on the phase variation deduced from ray-optics for the bispherical lens. It can be seen that the departures become more pronounced as the edges of the lens are approached. In effect the resolving power of the lens implied by its diameter cannot be realized. The possibility of using a full diffraction computation to explore the ramifications of ideal lens distortions will be discussed.

2.5 Forward Propagation

This section presents a development of what is usually referred to as the theory of diffraction by using only the plane-wave propagator. The formal equivalence between the Huygens-Fresnel integral representation and the FPE are

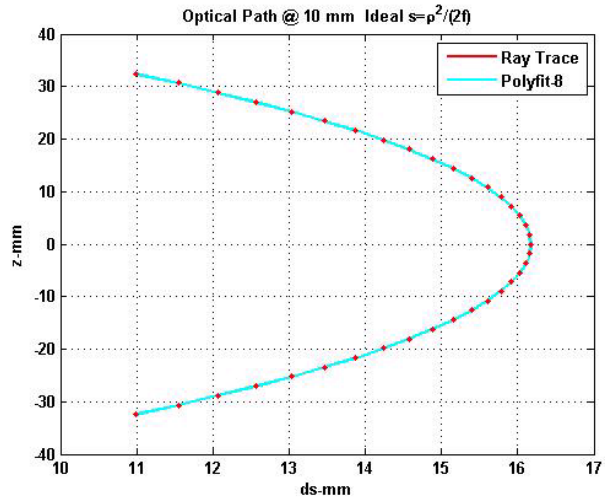


Figure 2: Optical path length computed from ray-trace (red dots) . Cuyan curve is least-squares fit to 8th order polynomial.

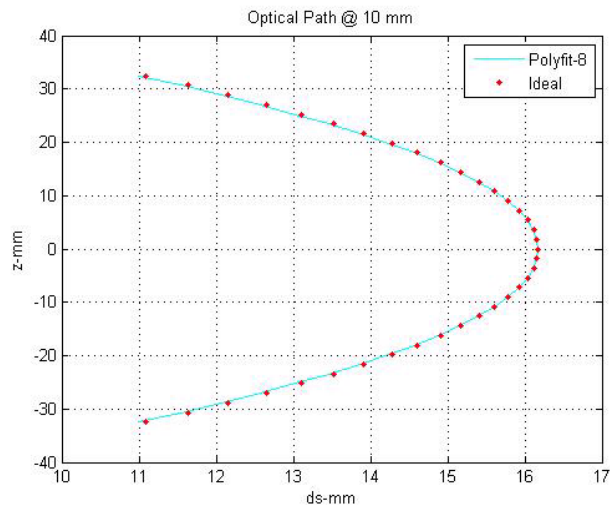


Figure 3: Ideal phase correction to produce a focus at a distance f from the aperture plane.

also demonstrated. The standard developments use the narrow-angle scatter approximation, whereas the Fourier-domain propagator requires no prior constraint.

2.5.1 Full-Wave Diffraction

In an unobstructed homogeneous region, the solution to the scalar Helmholtz equation is determined by the field in the plane at $x = x_0$, which will be referred to as the aperture plane. If the aperture plane is tilted, a linear phase variation can be applied to launch the wavefield normal to the orientation of the computation plane [6]. Alternatively, the propagator itself can be written for evaluation along the principal propagation direction [2, Chapter 4]. For the purposes of the development here, these details are unimportant.

If one is interested in the field only at a large distance from the aperture plane, the solution takes a particularly simple form. An application of the stationary phase approximation to (8) will show that

$$\lim_{\Delta x \rightarrow \infty} \Theta\psi(\Delta x, \varsigma) = -ig(\kappa_r) \left[k^2 \widehat{\psi}(0; \kappa_r) \right] \frac{\exp\{ikr\}}{2\pi kr}, \quad (22)$$

where $r = \sqrt{\Delta x + \varsigma^2}$ and κ_r is the transverse wavenumber in the direction of $\mathbf{r} = [\Delta x, \varsigma]$. It is fundamental to the design of remote sensing systems because it defines the on-axis signal intensity at distance r from the source. Off axis, the field variation is defined by the Fourier transform of the aperture distribution. In optics literature, (22) is called Fraunhofer approximation [5, Chapter 4]. Although the narrow-angle scatter approximation was not used in the derivation presented here, narrow-angle scattering is implicit because the transverse dimensions are necessarily small when $\Delta x \rightarrow \infty$.

The near-field is a much more demanding environment. To explore the near field, it is convenient to rewrite (8) as an explicit linear operation on the starting field:

$$\begin{aligned} \Theta\psi(x, \varsigma) &= \iint \left[\iint \psi(x_0, \gamma/k) \exp\{-i\boldsymbol{\eta} \cdot \boldsymbol{\gamma}\} d\boldsymbol{\gamma} \right] \\ &\times \exp\left\{i\sqrt{1-\eta^2}(k\Delta x)\right\} \exp\{i\boldsymbol{\eta} \cdot k\boldsymbol{\varsigma}\} \frac{d\boldsymbol{\eta}}{(2\pi)^2}. \end{aligned} \quad (23)$$

Changing the order of integration isolates the singular inner integral:

$$\begin{aligned} \Theta\psi(x, \varsigma) &\approx \iint \psi(x_0, \gamma/k) \\ &\times \left[\iint \exp\left\{i\sqrt{1-\eta^2}(k\Delta x)\right\} \exp\{i\boldsymbol{\eta} \cdot ((k\boldsymbol{\varsigma}) - \boldsymbol{\gamma})\} \frac{d\boldsymbol{\eta}}{(2\pi)^2} \right] d\boldsymbol{\gamma}, \end{aligned} \quad (24)$$

The exchange of integration order is justified when the spectral content of the starting field is limited to a narrow range of propagation angles, say where $\sqrt{1-\eta^2} \simeq 1 - \eta^2/2$. It then follows that

$$\begin{aligned}\Theta\psi(x, \varsigma) &\simeq \exp\{ik\Delta x\} \iint \psi(x_0, \gamma/k) \\ &\times \iint \exp\{-i\eta^2(k\Delta x/2)\} \exp\{i\eta \cdot ((k\varsigma) - \gamma)\} \frac{d\eta}{(2\pi)^2} d\gamma.\end{aligned}\quad (25)$$

The Fourier transform represented by the η integration can be evaluated analytically. Carrying out the integration leads to the following near-field form of the equation, which is called the Fresnel approximation

$$\begin{aligned}\Theta\psi(\Delta x, \varsigma) &\simeq \frac{-ik \exp\{ik\Delta x\}}{2\Delta x} \\ &\times \iint \psi(0, \varsigma'') \exp\left\{i(\varsigma - \varsigma'')^2 k / (2\Delta x)\right\} d\varsigma'' \\ &= \frac{-ik \exp\{ik\Delta x\}}{2\Delta x} \exp\{i\varsigma^2 k / (2\Delta x)\} \\ &\times \iint [\psi(0, \varsigma'') \exp\{i\varsigma''^2 k / (2\Delta x)\}] \exp\{-i\varsigma \cdot \varsigma'' (k/\Delta x)\} d\varsigma'',\end{aligned}\quad (26)$$

The two forms of the result are identical to Goodman's Equations (4-14) and (4-17). The fact that the final form of the Fresnel approximation is itself a Fourier transformation should not be confused with the Fourier transformation in the propagation integral (23), which involves no approximations.

The reason for rederiving these well know results here is to show that they are special cases of full-wave propagation, which can be evaluated numerically by using Fourier transformations. As already noted, there is no compelling reason to impose the narrow scatter approximation if numerical computation is being pursued. For the Fraunhofer regime, this is empty generality because there are few, if any, practical situations where the narrow-angle scatter approximation is violated. This is manifestly not the case in the Fresnel region. To explore this, consider the Huygens-Fresnel construction, which is also exact insofar as the propagation of a known starting field is concerned. The main difference is that the Huygens-Fresnel starting field is defined on a non planar surface.

Starting with Huygens-Fresnel, consider the field in a plane at $x = x_0$ that isolates the defining surface from an unobstructed propagation space. From (6),

$$\psi_{HF}(x_0, \varsigma) = \iint_{\Sigma} U(\mathbf{r}_s) \frac{\exp\{ik|x_0 - x_s, \varsigma - \varsigma_s|\}}{|x_0 - x_s, \varsigma - \varsigma_s|} ds. \quad (28)$$

Substituting the Wyle representation of the Green function,

$$\frac{\exp\{ik|\Delta x, \varsigma - \varsigma'|\}}{|\Delta x, \varsigma - \varsigma'|\} = \iint \frac{i \exp\{ikg(\kappa)\Delta x\}}{2kg(\kappa)} \exp\{i\kappa \cdot (\varsigma - \varsigma')\} \frac{d\kappa}{(2\pi)^2}, \quad (29)$$

into (28) and reversing the order of integration as before shows that

$$\begin{aligned}
\psi_{HF}(x, \varsigma) &= \iint_{\Sigma} U(\mathbf{r}_s) \iint \frac{i \exp\{ikg(\kappa)\Delta x\}}{2kg(\kappa)} \exp\{i\kappa \cdot (\varsigma - \varsigma_s)\} \frac{d\kappa}{(2\pi)^2} ds \\
&= \iint \left[\frac{i}{2kg(\kappa)} \iint_{\Sigma} U(\mathbf{r}_s) \exp\{-i\kappa \cdot \varsigma_s\} ds \right] \exp\{i\kappa \cdot \varsigma\} \\
&\quad \times \exp\{ikg(\kappa)\Delta x\} \frac{d\kappa}{(2\pi)^2}. \tag{30}
\end{aligned}$$

Evaluating the two-dimensional Fourier transform of $\psi_{HF}(x_0, \varsigma)^3$ establishes the equivalence

$$\widehat{\psi}_{HF}(x_0, \kappa) = \frac{i}{2kg(\kappa)} \iint_{\Sigma} U(\mathbf{r}_s) \exp\{-i\kappa \cdot \varsigma_s\} ds. \tag{31}$$

Rewriting (30) in terms of $\widehat{\psi}_{HF}(x_0, \kappa)$ reproduces the plane-wave propagator:

$$\psi_{HF}(x, \varsigma) = \iint \widehat{\psi}_{HF}(x_0, \kappa) \exp\{ikg(\kappa)\Delta x\} \frac{d\kappa}{(2\pi)^2}. \tag{32}$$

Note that (31) defines the Fourier transformation as an integration over the induced sources of the field. It shows as well that the subsequent propagation of that field can be calculated in principle without approximation using Fourier-domain methods. The factor $1/g(\kappa)$ in (31) is singular at $k = \kappa$. For $k < \kappa$ it has little effect, but to properly accommodate the singularity requires careful evaluation. The poles in the spatial Fourier domain are necessary for generating the singular behavior of the Green function. With the singular points in the source region well removed from the plane at $x = x_0$, this term can be safely ignored.

Reciprocity provides another example of the equivalence between Green-function and plane-wave representations. The Green function is intrinsically symmetric to an interchange of the source and field point variables, which leads to the reciprocal interchange between a source point and a measurement point. It is also true that a spectral domain representation that maps incident plane waves to forward or scattered plane waves can be constructed for invariance to an interchange of wave vectors. [7].

3 Numerical Examples

There are two integral representations of a propagator that can be used for computing the free-space evolution of a starting field. To the extent that the computation is to be done numerically, sampling requirements dictate the most

³ $\Delta x = 0 \Leftarrow x = x_0$

efficient method. If finite-difference methods are used, the diffraction operator must be approximated. This can be advantageous if the spatial-domain support of the field is constrained.

3.0.2 Fraunhofer Diffraction

The first example uses a zero-phase starting field defined in a plane. A uniform circular “top hat” is a convenient realization because it admits an exact transform:

$$\begin{aligned}\widehat{\psi}(x_0, \kappa) &= \iint_{-D/2}^{D/2} \exp\{-i\zeta \cdot \kappa\} d\zeta \\ &= \int_0^D \zeta \int_0^{2\pi} \exp\{-i\kappa\zeta \cos \phi\} d\phi d\zeta \\ &= \frac{2\pi}{\kappa^2} \int_0^{\kappa D} \eta J_0(\eta) d\eta = \frac{2\pi D}{\kappa} J_1(\kappa D).\end{aligned}\tag{33}$$

From (27), the field in the focal plane of a lens is

$$\psi(f, \varsigma) \sim \frac{2\pi f D}{k\varsigma} J_1(k\varsigma D/f).$$

The standard estimate of the focal spot size

$$d = 1.22\lambda f/D,\tag{34}$$

follows [5, Equation (4-32)].

Consider a uniform circular 0.46μ source with diameter $D = 68.56$ mm, which is the maximum extent of the lens used in the ray-trace example. Standard discrete Fourier transform (DFT) sampling requirements establish the relation

$$\Delta L \Delta K = \frac{2\pi}{N}.$$

Since the power-spectrum of the complex wavefield is invariant to propagation, the source field determines the sampling interval. In the far-field the beam will expand at a rate dictated by the angular extent of the Fourier-transform of the disc normalized to wavenumber. Since the expanding beam must stay within the computation grid to minimize edge effects, a span of $5D$ was used to accommodate a propagation distance of $10 m$. Note that although $D/\lambda = 1.5 \times 10^5$, adequate sampling was achieved on a 4096×4096 grid with $\lambda/dy = \lambda/dz = 364$.

Figure 4 shows a the vertical plane intensity for 50 logarithmically spaced propagation steps. The field has been normalized to its on-axis peak, which

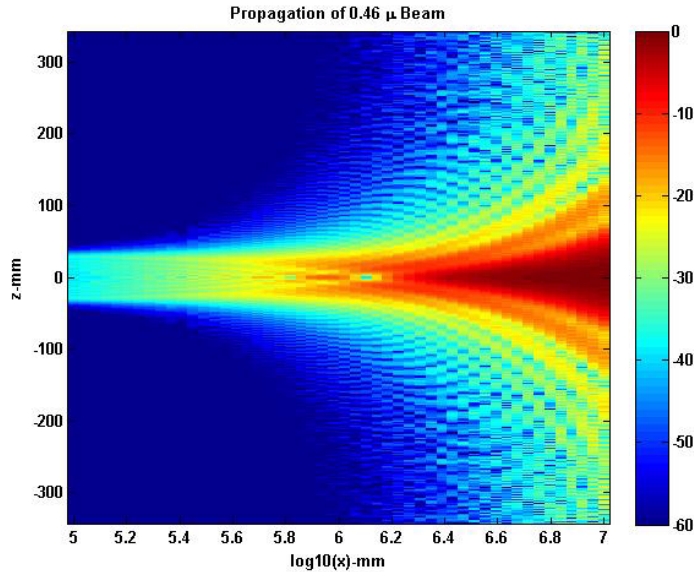


Figure 4: FPE computation of the forward propagation of an unfocused circular spot. The field intensity is a vertical slice of the two-dimensional field multiplied by the square of the propagation distance.

becomes constant when the Fraunhofer limit is achieved. Logarithmic propagation steps were used to capture the evolution from the near field to the far-field limiting form. One can verify that the sidelobes are predicted by the Fourier transform of the disk. The point-spread function in the focal plane of a lens (27) has this same overall shape.

Each computation step requires forward and inverse DFTs with intervening matrix multiplication. The computation used approximately 20 s per step on a 64-bit, dual-processor PC with 8 GBytes of memory.

If one were interested only in free-space propagation, the computation of the far-field limit would be of academic interest. However, if the propagation medium is structured, the split-step method accommodates the effects of the structure without further approximation.

3.0.3 Fresnel Diffraction

Computation of Fresnel diffraction in the absence of high curvature are well established [5, Section 4.5]. Zeng and McGough demonstrated the full-wave propagator for a low-curvature acoustics application [8]. The more challenging application is the focusing of the wave field as it propagates from the plane of a lens system aperture stop. Although ray-optics could be used to estimate the

focal plane field, the simpler top-hat form with an appropriate phase variation will be used here. The spherical wave to aperture distance might be used as a surrogate:

$$\psi(\zeta) = \exp \left\{ ikf \left(1 - \sqrt{1 - \zeta^2/f^2} \right) \right\} \text{ for } \zeta < D/2. \quad (35)$$

On the other hand, the Fresnel approximation shows that an aperture distribution with quadratic phase, namely

$$\psi(\zeta) = \exp \{ ik\zeta^2 / (2f) \} \text{ for } \zeta < D/2, \quad (36)$$

is consistent with the Fourier-transform relation between the uniform aperture and the focal-plane PSF. The aperture fields (35) and (36) are nearly equal for large f/D ratios.

Sampling requirements here are driven by the extreme phase variation at optical frequencies ($k > 10^5$). It should not be surprising that near-wavelength sampling is necessary. Trial and error showed that sampled fields similar to the Fraunhofer example could be used only for wavelengths in the millimeter range. The focal length and aperture size were adjusted to provide a large aperture in wavelengths.

To demonstrate the sampling requirements, Figure 5 shows the focal-plane spectral density plotted against wavenumber normalized by k . An aperture diameter of 60 mm was used with $k = 10$ reciprocal millimeters ($f = 477.5$ GHz). The quadratic source field defined by (36) with $f = 140$ mm was used. The computation shows that the significant portion of the spectral intensity occupies nearly 50% of the range of non-evanescent waves, which is well beyond narrow-angle scatter limits.

With adequate sampling, the field in any forward plane can be computed by applying the Fourier-domain propagator. Figure 6 shows a vertical-plane cut of the field intensity computed over 111 planes centered on the nominal focal distance with 1-mm spacing. The x distance is measured from the exit plane, which accounts for the displacement of the focus from 140 mm. Figure 7 shows the detail of the Focal plane intensity. It is imperceptibly different from the scaled Fourier transform of the Fourier-transform of the aperture stop as predicted by (27).

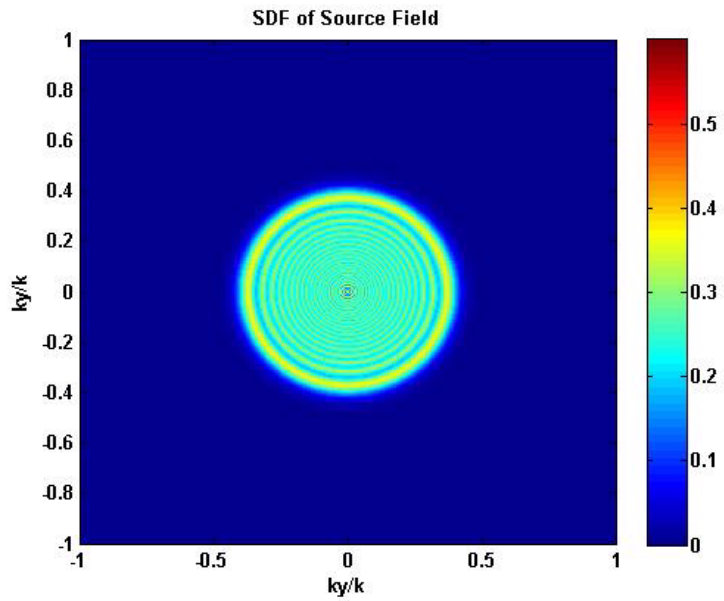


Figure 5: Spectral density function plotted against normalized spatial wavenumber for quadratic-phase starting field.

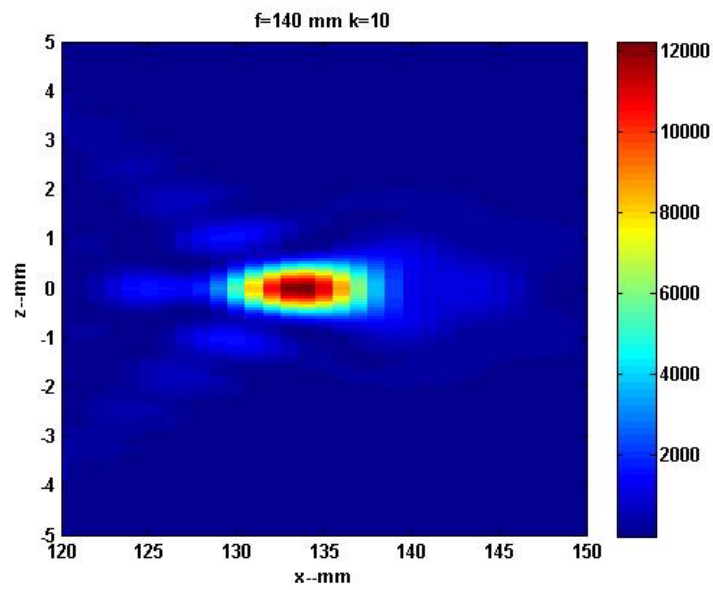


Figure 6: Evolving field in vertical plane slice through the focal point.

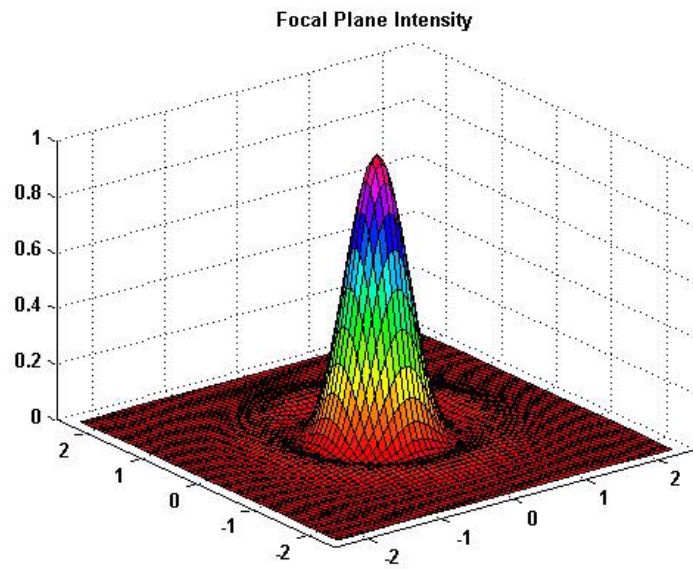


Figure 7: Focal plane field intensity.

4 Summary and Conclusions

In Section 2.5.1 showed that the full-wave diffraction operator contains within it the Fraunhofer and Fresnel approximations and the Fourier transformation relation between the aperture field and the focal plane distribution of the field. A varying refractive index can be accommodated, which supports ray optics as a geometric construct for evaluating field structure. However, to use the diffraction operator for propagation computations, it is necessary to determine the starting field in the boundary plane. Choosing an appropriate starting field is a topic well covered in the PWE literature. Within the confines of the narrow-angle scatter approximation, the PWE formalism and the full diffraction approach are indistinguishable, and the equivalences established are of purely academic interest.

The most challenging computation is the propagation of a converging spherical or near spherical wavefront to a focus. Ray optics can be used to accurately predict where the focus will occur, and its degree of definition; however, the field in the vicinity of the focus requires diffraction theory. The Huygens-Fresnel construction will accurately compute the field near the focus, but in the intervening region the computation, although feasible, is much more demanding. In principle, the diffraction operator can be used to propagate the field from the aperture plane through the focus and beyond. This was demonstrated with a 477.5 GHz field. This was the highest frequency for which the computation could be performed on a high-end PC without memory management. One may recognize that the computation is equivalent to evaluating the diffraction integral beyond the limits of the Fresnel-integral. The same problems occurs in trying to compute the Fourier transform of a quadratic chirp radar signal. In any case, we believe that the use of the exact form of the plane-wave propagation operator is both satisfying as an exact presentation of diffraction theory and possibly a new method of calculating Fresnel domain fields.

Acknowledgement

The assistance of Dennis Hancock in clarifying concepts and optical methodology is gratefully acknowledged. <http://dennishancock.com/>

References

- [1] J. A. Kong. *Electromagnetic Wave Theory: Second Edition*. John Wiley & Sons, New York, 1986.
- [2] Charles L. Rino. *The Theory of Scintillation with Applications in Remote Sensing*. John Wiley and Sons, Inc., New York, 2011.
- [3] Mireille Levy. *Parabolic Equation Methods for Electromagnetic Wave Propagation*. Institute of Electrical Engineers, United Kingdom, 2000.
- [4] M. Born and E. Wolf. *Principles of Optics*. Cambridge University Press, 1999.
- [5] Joseph W. Goodman. *Introduction to Fourier Optics*. Roberts and Company, Connecticut, 2005.
- [6] N. Delen and B. Hooker. Verification of comparison of a fast fourier transform-based full diffraction method for tilted and offset planes. *Applied Optics*, 40(21):3525–3531, 2001.
- [7] Hoc D. Ngo and Charles L. Rino. Wave scattering functions and their application to multiple scattering problems. *Waves in Random Media*, 3(3):199–210, 1993.
- [8] Xiaozheng Zeng and Robert J. McGough. Evaluation of the angular spectrum approach for simulations of near-field pressures. *J. Acoust. Soc. Am.*, 123(1):68–76, 2008.